

Drop-on-demand satellite-free drop formation for precision fluid delivery

Lisong Yang¹, Nik Kapur², Yiwei Wang², Fritz Fiesser³, Frank Bierbrauer², Mark C. T. Wilson²,
Tim Sabey⁴ and Colin D. Bain^{1†}

¹Department of Chemistry, Durham University, Stockton Road, Durham, DH1 3LE, UK

²School of Mechanical Engineering, University of Leeds, Leeds, LS2 9JT, UK

³GlaxoSmithKline, Collegeville, Philadelphia, PA 19426, USA

⁴GlaxoSmithKline, Barnard Castle, Co. Durham, DL12 8DT, UK

[†] Email address for correspondence: c.d.bain@durham.ac.uk

Abstract

A drop-on-demand liquid dispensing system, based on a rotary piston pump, for delivering microlitre droplets at ~ 10 Hz is analysed. Five types of drop formation are observed under different pump operation schemes, characterised by the breakup behaviour of the thin liquid ligament that develops between the forming drop and the liquid remaining at the dispensing nozzle. A range of control parameters and fluids (Newtonian and non-Newtonian) have been explored in order to identify key system parameters for precise satellite-free drop formation and hence to establish an operating window. Under a conventional ‘one-step-ejection’ pump operation cycle, the window for satellite-free drop production is found to be small and impractical due to the long ligament and large pendant drop at the nozzle. The satellite-free operating window can be expanded dramatically with the ligament and pendant drop size under control with a novel ‘two-step-ejection’ process, in which the drop is first partly grown, then allowed to settle, and then ejected via a second pulse of liquid from the pump. Rapid deceleration of the pump near the maximum flow rate at the end of the second pulse is essential for satellite-free drop production.

Key words: Drop-on-demand, satellite, flow rate, Newtonian and Non-Newtonian fluid, digital printing

1. Introduction

The formation of drops from streams of liquid has fascinated natural scientists for centuries. In the drop formation process, the physical parameters of the liquid (interfacial tension and rheology), the geometry of the nozzle and process parameters (flow rate, ejection profile, body forces) interact to control the highly non-linear droplet formation process. Consequently such processes have received great interest from the academic community. The formation of drops has also been widely applied in production of microarrays, fabrication of transistors, protein crystallography, inkjet printing, and maskless lithography since it offers the ability to repeatedly generate controlled volumes of fluid (Martin, Hoath & Hutchings 2008; Gamerith et al. 2007; Beecher et al. 2007; Basaran 2002; Ng et al. 2007; Sumerel et al. 2006). There are two main drop formation modes: a continuous mode operating under a constant flow (dripping and continuous jetting) and drop-on-demand (DOD) mode under a pulsed flow. The former process has been studied for over a century and the vast literature has been well reviewed (Subramani et al. (2006); Eggers (1997; 2005)). DOD jetting is, by comparison, a relatively new technique which was invented by Zoltan (1972) and Kyser and Sears (1976) in which a discrete pressure pulse is applied upstream of a nozzle of a few tens of microns in diameter through which the drop (picolitres in volume) is ejected. Fromm (1984) simulated the DOD process using a marker-and-cell method and subsequently a number of investigators developed numerical methods with improved accuracy (Xu and Basaran 2007 and references therein).

Although the driving force of drop formation in continuous and DOD modes is different, there is a phenomenological similarity in the drop breakup. In all cases, the length of a liquid ligament that connects the nascent drop to the remainder of the liquid increases as its diameter decreases due to a combination of capillary forces and body forces (principally gravity). The ligament eventually pinches off and a free drop forms. The liquid thread can break off at multiple locations and result in the production of one or more small satellite droplets. Satellite droplets are undesirable in most manufacturing applications due to the uncertainty in the position of their final deposition. In the

continuous mode, the satellite droplets can be eliminated by applying a large perturbation upstream of the nozzle – frequently a sinusoidal wave, allowing control over amplitude and wavelength (Pimbley & Lee 1977) – or by excitation with combinations of harmonics (Chaudhary & Maxworthy 1980). In the case of DOD, finding the working conditions for the suppression of satellites for viscous fluids remains a trial-and-error process for the formation of both microlitre (Castrejón-Pita et al. 2008, 2011; Harris et al. 2015) and picolitre drops (Wang et al. 2012; Dong, Carr & Morris 2006; Kwon 2010). Castrejón-Pita et al. (2015) fitted a nozzle with an iris to allow variation of the nozzle diameter in their μL -drop generator in order to control the number of satellites. Their results suggest a strong correlation between the conditions required to eliminate the satellite droplet and the drop volume, which could limit the flexibility to create drops of pre-defined size.

Whilst industrial application of precision droplet delivery has largely been in dispensing pL volumes of fluid, the convenience of being able to deposit larger droplets accurately (10's of μL) offers new manufacturing opportunities – for example in printed pharmaceuticals (Clarke et al. 2013) where doses are in the milligram range and consequently there is a demand for larger carrier droplets. The criteria for control of the printing process are the same as in conventional inkjet – namely repeatable droplet volumes without satellites, operation in a DOD mode, and precise control of drop volume.

This paper addresses the design and underlying behavior of a drop delivery system for μL drops using a piston pump. In developing a large-volume DOD method, a wide range of parameter space has been studied and from these data conclusions have been drawn that illustrate the salient features of the process. We observed five types of drop formation under different pump operation schemes (see figure 1 and the movies) defined by how the ligament pinches off. For ease of description, we refer to the end of the ligament attached to the forming primary drop as the *fore* end, and the end attached to the remaining pendant liquid at the nozzle as the *aft* end. The five modes of drop break-off observed are: 1) the ligament pinches off at the *fore* end first and then the *aft* end with an elongated rear that recoils into a backward-moving satellite droplet that

eventually merges into the pendant drop (type-FA drop formation, figure 1a and movie 1); 2) the break-offs occur at both ends of the ligament almost *simultaneously*, creating a long-lived satellite (type-S drop formation, figure 1b and movie 2); 3) the ligament breaks off at the *aft* end first and then the *fore* end, forming a forward-moving satellite that merges into the primary drop (type-AF drop formation, in figure 1c and movie 3); 4) the ligament pinches off only at the *aft* end therefore no satellite forms (type-A drop formation, figure 1d and movie 4); and 5) the ligament pinches off only at the *fore* end producing no satellite (type-F drop formation, figure 1e and movie 5). These phenomena were observed in both Newtonian fluids and a shear-thinning suspension chosen as a model system inspired by an industrial application. Satellite production (type-AF, type-FA and type-S) is undesirable since the satellites reduce control over drop volume, accumulate on process equipment reducing performance, and can be a health hazard. In type-FA and type-AF drop break-off, the satellite would ideally be absorbed by the pendant drop or the primary drop, respectively. However performance is vulnerable to environmental factors (such as air flows caused by the movement of the substrate or print head) that can cause the satellite to be deposited away from the primary drop. We show below that type-A drop formation is preferable to type-F since there is a larger operability window, a shorter break-off length (defined as the length of the pendant drop measured from nozzle plate to its tip at the first pinch-off) and hence a lower stand-off between nozzle and substrate, and a smaller pendant drop left attached to the nozzle.

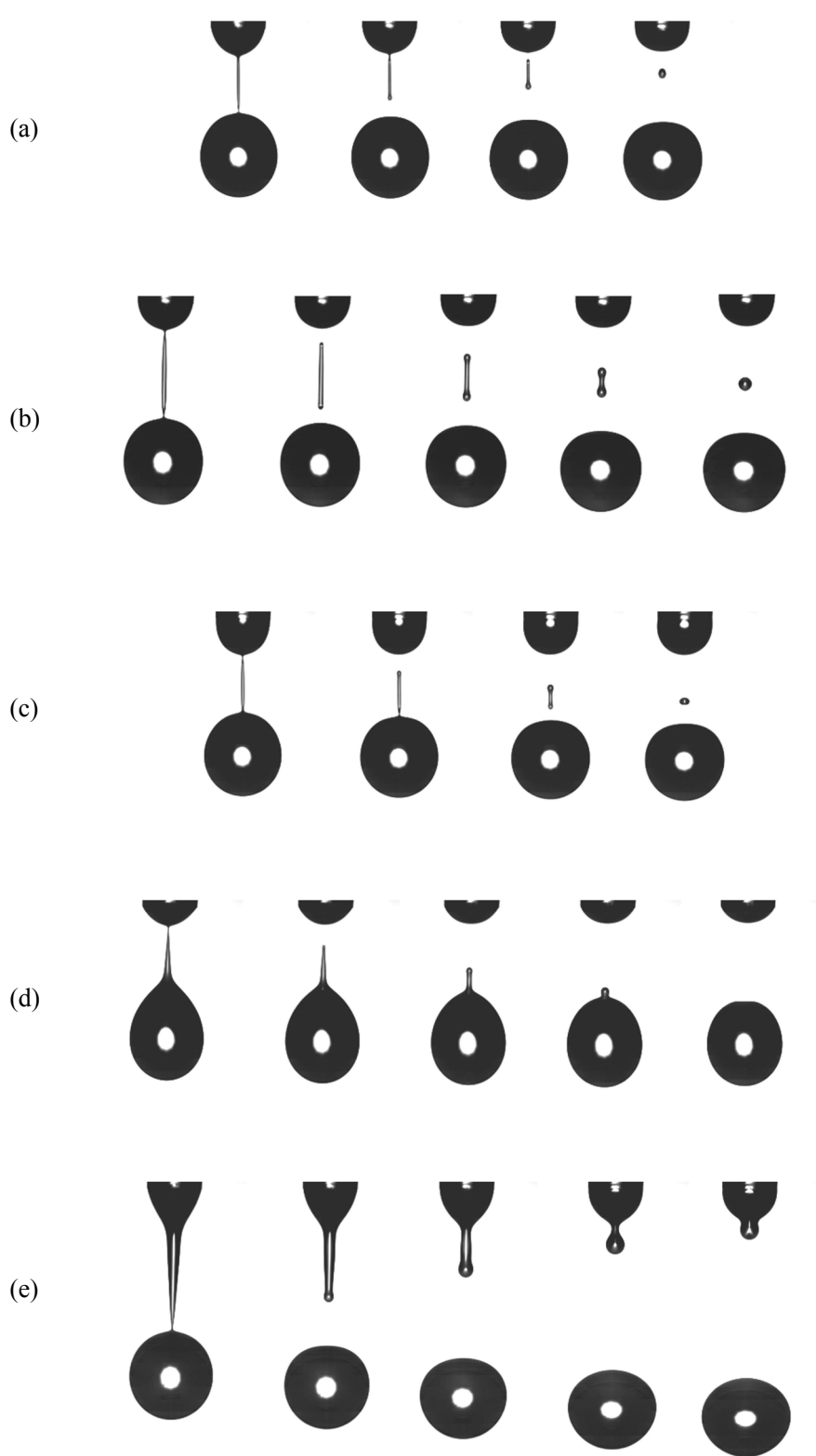


Figure 1. Five types of drop break-off classified by the order in which ligament rupture occurs (F = fore, A = aft, S = simultaneous): (a) FA, (b) S, (c) AF, (d) A, (e) F.

2. Experimental setup

2.1 DOD dispensing system based on a piston pump

The experimental setup for DOD dispensing of μL drops has been described in detail elsewhere (Yang et al. 2014; Clarke et al. 2013). The central component of the system is a rotary piston pump head (IVEK -3A). A single revolution consisting of a fill and discharge cycle is illustrated in figure 2. A close-fitting piston sits within a cylinder. The piston is simultaneously displaced back and forth (controlling the pressure within the pump - either a low pressure to fill or a high pressure to discharge) and rotationally (controlling the opening of either the inlet port during filling or outlet port during discharge). The frequency of rotation, ω , controls the number of pump cycles per second and the volume discharged per cycle is controlled by the length of piston travel within the bore (adjusted mechanically). A dial gauge was mounted on the pump head allowing repeatable setting of the stroke volume in the range 5–30 μL . Repeatability of 0.1% is obtainable once the stroke volume is set. The rotation and displacement are mechanically coupled. The linear displacement of the piston l_{piston} is given by $(1 - \cos \theta) L_{\text{stroke}}/2$, where L_{stroke} is the maximum length that piston travels, i.e. stroke length, and θ is the piston rotary angle, where $\theta = 0$ is defined at its top dead center, shown in figure 2c. The discharged fluid volume V as a function of θ is given by

$$V = \frac{\pi D_{\text{piston}}^2 l_{\text{piston}}}{4} = \frac{\pi D_{\text{piston}}^2 L_{\text{stroke}}}{8} (1 - \cos \theta), \quad (2.1)$$

where D_{piston} is the diameter of the piston (3.15 mm for the pump head used here) and for a constant angular velocity ω , where $\theta = \omega t$, the flow rate, Q , is given by

$$Q = \dot{V} = \frac{\pi D_{\text{piston}}^2 L_{\text{stroke}}}{8} \omega \sin \theta \quad (2.2)$$

By way of confirmation of equation. 2.1, the movement of the water meniscus up a fine-bore glass capillary during the pump discharge phase was measured as a function of rotary angle, shown in figure 3 (dotted line). This shows good correlation between equation 2.1 (solid line) and the experimental measurement, with some small deviations near the extrema of the piston movement, possibly due to the mechanical design of the pump outlet. The experimental data can be well fitted with a cubic polynomial. The fitting parameters are used below to convert pump position into discharged volume.

The calibration curve in figure 3 can be scaled for different stroke volumes.

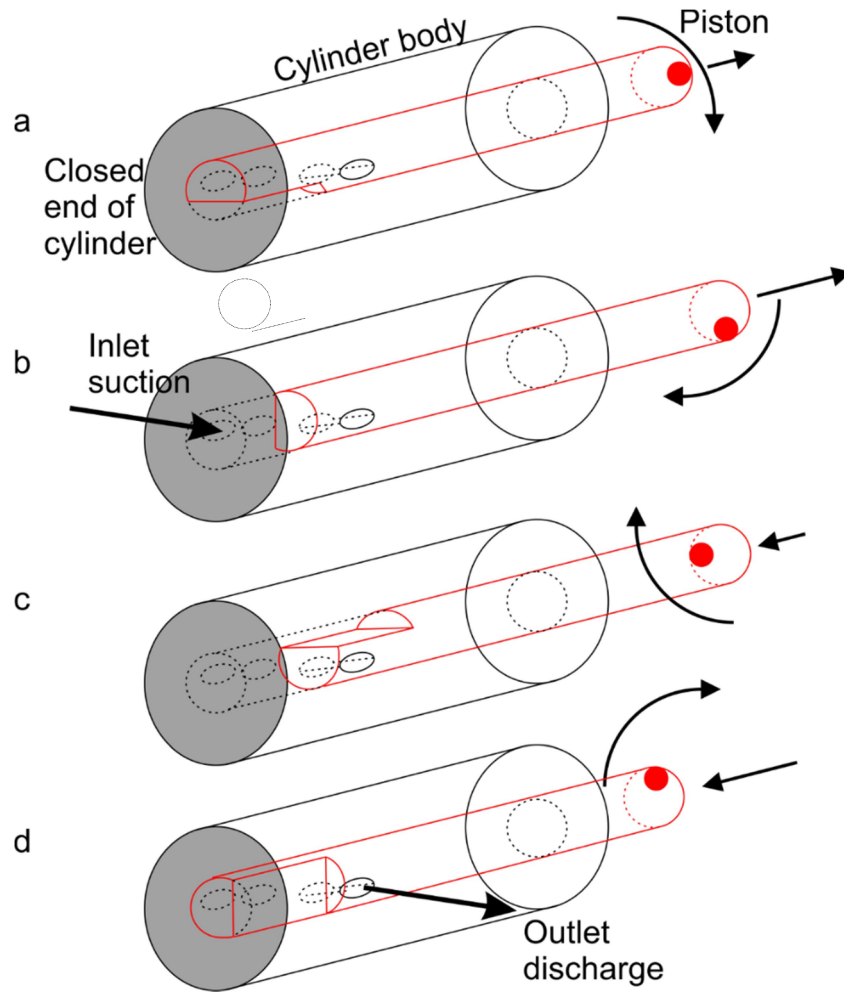


Figure 2. (Color online) Mechanism of IVEK rotary piston pump with (a) the piston is at the bottom dead centre of its stroke ($\theta = 180^\circ$). Both inlet and outlet ports are closed, (b) the piston simultaneously retracts and rotates within the cylinder, through the use of a swash-plate that couples the drive motor to the piston. The piston flat opens the inlet port and draws fluid into the pump chamber (noting that the outlet port remains closed), (c) the piston retracts further towards its top dead centre of the stroke, where the pump chamber is fully filled ($\theta = 0^\circ$). Both inlet and outlet ports are closed, and (d) the piston flat rotates towards the outlet port creating a discharge path and as the piston advances inside the cylinder, fluid is discharged from the cylinder. The piston further advances to the bottom dead centre (a) and cycle repeats. The inlet port is closed in the discharging phase.

The pump head was coupled to a servo motor (Allen-Bradley, MPL-A230) fitted with an accurate encoder allowing the absolute position to be determined, which in turn was

driven by a digital servo drive (Allen-Bradley, Ultra3000) allowing fine control of the motor. Software (Allen-Bradley, Ultraware) allows a user-defined pump profile (angular velocity) to be set over one revolution, giving the control required to investigate the effect of complex flow profile in time on the drop formation process. The actual position from the motor can also be captured, allowing the actual pump profile to be recorded.

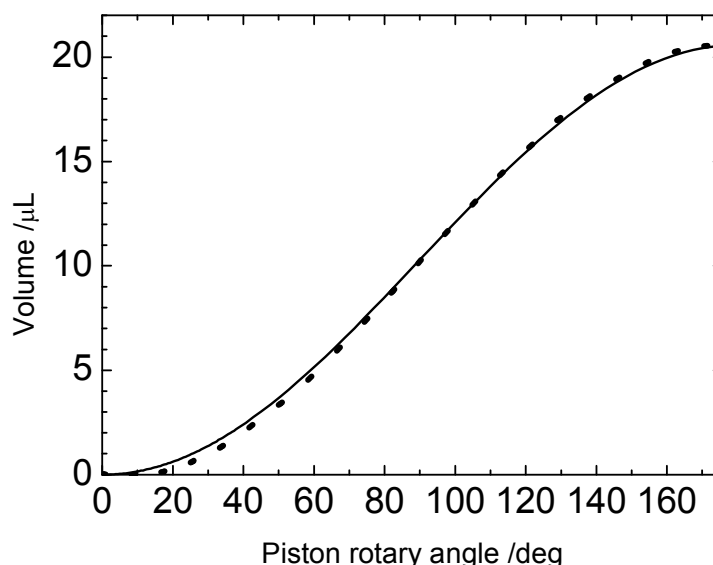


Figure 3. Experimental data (dotted line) and calculated values from equation 2.1 (solid line) of the dispensed volume as a function of the piston position.

The resulting pump system was coupled between a reservoir of the test fluid and a nozzle cut from a section of PTFE tubing (Zeus), with a sharp right angle cut perpendicular to the long axis of the tube. AWG15 sized tubing is used in the experiments with an inner diameter of 1.45 ± 0.05 mm and outer diameter of 2.25 ± 0.05 mm.

For efficient delivery, it is desirable that one rotation of the pump ejects one drop (defined here as detached fluid containing a primary drop plus any satellites). The motor control parameters, mainly the ejection rate and volume of ejection, are matched with the size of the tubing to discharge a single drop during each pump stroke. For a given tubing and stroke volume, there exists a lowest ejection rate, i.e. a critical point, above which one stroke generates one drop. The stroke volume in the experiments described

below was 18.8 μL except where otherwise specified.

We note that cavitation can occur during the pump suction phase. Cavitation during filling of the pump results in a reduction in the discharge volume. A more viscous fluid creates a larger pressure drop over the pump inlet and shows an earlier onset of cavitation than a less viscous fluid under the same running conditions. In all experiments reported here, cavitation is avoided by controlling the filling rate.

2.2 Visualisation and image analysis

Shadowgraphs of the drop are obtained with back illumination. A Leica CLS 100 \times illuminator is used as a light source. The light is collimated through a singlet lens with a focal length of 80 mm with a clear aperture of 20 mm. Two visualisation approaches are used to trace the formation of the fast-moving drop: a stroboscopic imaging technique and a high-speed camera. For the strobe image, a TTL signal generator is used to trigger the Ultra3000 servo drive directly and a Jai M10SX CCD camera through a delay circuit. The shortest exposure time of the camera is 1 μs . The resolution of the delay box is 0.2% of its range (either 2, 20 or 200 ms). For a fixed delay, a pseudo-frozen image of the drop at a specified position in the ejection cycle can be visualised and quantified. It is a practical tool to monitor the drop reproducibility in real-time. To obtain a time series of images from a single droplet we use a high-speed CMOS camera (Photron FASTCAM-APX RS). The typical image size is of 400×1024 pixels with a resolution of 20 $\mu\text{m}/\text{pixel}$ and a frame rate of 2000 fps (videos are replayed at 30 fps). The camera is triggered via software. The output TTL signal from the camera is sent to the motor drive to start the pump. The drop formation is analysed through Matlab code with an edge detection algorithm using a Sobel operator. The volumes of pendant, primary and satellite drop are calculated with an assumption that the drop is axisymmetric.

2.3 Sample preparation and physical characterization

We have studied both Newtonian solutions and an aqueous colloidal suspensions exhibiting non-Newtonian behaviour. The Newtonian solutions were prepared with 4 wt%, 5.6 wt% and 6 wt% hydroxypropyl cellulose (HPC-sl, Nisso, $M_w \sim 100,000 \text{ g mol}^{-1}$

¹) dissolved in water. The colloidal suspension was formulated from a binder (hydroxypropyl cellulose, HPC-ssl, Nisso, average molecular weight $M_w \sim 40,000$ g mol⁻¹), a suspending agent (fumed silica, DHK SiN20, Wacker), a dispersant (Tween 80, Aldrich) and 9,10-anthraquinone (AQ) (Alfa Aesar) with a density of ~ 1500 kg m⁻³ and very low solubility in water (~ 1 mg/L) as an analog for a typical active pharmaceutical ingredient (API). AQ was micronised by an air-jet mill to give a final size < 10 μ m measured by MasterSizer (Malvern 2000). All experiments in this paper were executed at room temperature of 21 ± 1 °C.

An AR 2000 rheometer (TA instrument) with a cone-on-plate geometry (plate diameter = 60 mm, cone angle = 2°) was used to measure the steady-state shear viscosity of aqueous samples as a function of shear rate. The equilibrium surface tension, σ_{eq} , of Newtonian samples was measured by drop-shape analysis (FTA 200, First Ten Ångströms). The density of all samples was measured using a calibrated density bottle.

TABLE I shows the average shear viscosity over the shear rate of 1–1500 s⁻¹, the equilibrium surface tension and the density of the solutions. The viscosity of the cellulose solutions was almost independent of shear rate with an absolute variation of < 0.7 mPa s, thus demonstrating Newtonian behaviour over the range of investigated shear rates.

TABLE I. Measured physical properties of cellulose solutions with different concentration. Compositions are given in wt% in water.

Sample	μ / mPa s	σ_{eq} / mN m ⁻¹ ^a	ρ / kg m ⁻³ ^b
4% HPC-sl/W	18	44.5	1005
5.6% HPC-sl/W	32	44.5	1008
6% HPC-sl/W	45	44.5	1009

^a ± 0.5 mN m⁻¹; ^b ± 2 kg m⁻³

Two colloidal suspensions, AQ-20/W and AQ-33/W, were prepared with the weight percentages of each component listed in Table II. The detailed preparation of the colloidal suspension has been described elsewhere (Yang et al. 2014). The colloidal suspensions are shear-thinning fluids with the viscosity of AQ-20/W at high shear (1500

s⁻¹) matching that of the Newtonian system. The shear viscosity of the colloidal suspensions at shear rates of 0.1 and 1500 s⁻¹ and their density are listed in Table II. Figure 4 shows the shear viscosity of the colloidal suspensions alongside the data for the Newtonian system (5.6 wt% HPC-sl). The dynamic surface tension (DST) of AQ-20/W measured by the oscillating drop method (Yang et al. 2014) is 47 mN m⁻¹ at the surface age of ~ 30 ms. For the AQ-33/W the damping of the oscillation was too fast to permit measurement of the oscillation frequency.

TABLE II. Shear viscosity, μ , and density, ρ , of the colloidal suspensions.

Compositions are given in wt% in water.

Sample	HPC-ssl	SiN-20	Tween 80	AQ	$\mu @ 0.1 \text{ s}^{-1} / \text{mPa s}$	$\mu @ 1500 \text{ s}^{-1} / \text{mPa s}$	$\rho / \text{kg m}^{-3} \text{ }^a$
AQ-20/W	4.2	1.7	0.42	20	8500	34	1085
AQ-33/W	2.8	1.6	0.39	33	18000	180	1130

^a $\pm 2 \text{ kg m}^{-3}$

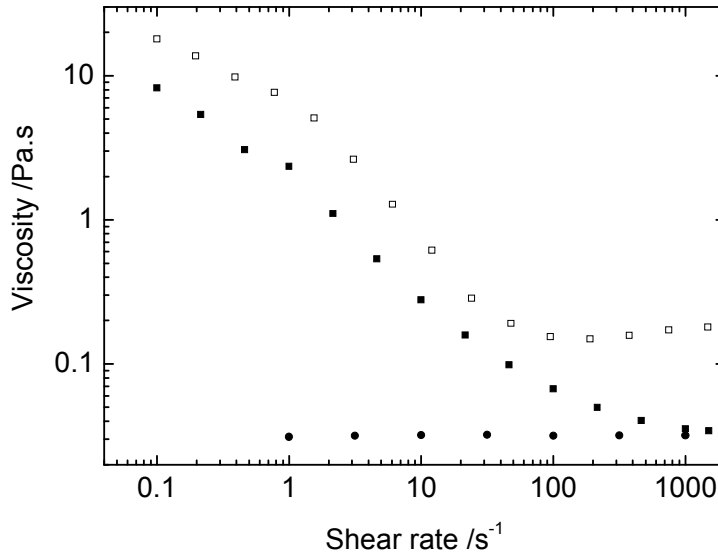


Figure 4. Shear rate dependence of viscosity on AQ-20/W (solid square), AQ-33/W (open square) and 5.6% HPC-sl/water (circle).

3. Drop formation under conventional pump cycle

The simplest profile for droplet ejection is to run the pump under constant angular velocity. During discharge, the flow rate Q will be a sinusoidal flow given by equation 2.2. For a DOD system, this pump profile is modified such that the droplet ejection

consists of three phases: pump filling (F), dwell (D) and ejection (E). We name this profile one-step-ejection (OSE). In DOD mode, the filling rate is independent of discharge, allowing faster filling for low viscosity fluids and a corresponding reduction in cycle time, or slower filling for more viscous fluids to avoid cavitation. A small modification is required in that the acceleration and deceleration are finite due to the dynamics of the system. Figure 5 shows a typical set of curves describing the behaviour of the pump using feedback from the position sensor: angular velocity, angular position, discharged volume and flow rate. The discharge flow rate is similar for continuous motion and the DOD profile (a sinusoidal wave) and the flow rate reaches its maximum near the middle of the ejection process, shifted in time for the DOD case owing to the pause between fill and discharge. The motor acceleration for the DOD case occurs at the start of the pump discharge where the rate of fluid ejection is small (see figure 3).

Figure 6 illustrates the drop formation for 5.6% HPC-sl under both constant pump speed (figure 6a) and DOD pump cycle (figure 6b) and for AQ-20/W under DOD profile (figure 6c). In all cases, the pump ejection rate is just above its critical point, that is one stroke generates one drop, and the stroke volume is $18.8 \mu\text{L}$. These fluids have the same viscosity at a high shear rate of 1500 s^{-1} . Under a constant pump speed, the long ligament in 5.6% HPC-sl breaks simultaneously at both ends (within the time resolution of 0.3 ms), i.e. type-S drop formation, and the resulting satellite droplet does not merge with either the residual pendant fluid or primary droplet. The two fluids show very similar behavior under the DOD profile. Although the low-shear rheology of the two fluids is very different (Fig. 4), at the point of discharge the rheological properties are similar due to the high shear experienced during flow through the pump and the nozzle, which is discussed in section 4.6. Both fluids form a long ligament that breaks first at the *fore* end and then at the *aft* end with an interaction time of 1 ms (that is the time between rupture of the two ends of the ligament). In this case the resulting satellite droplet then merges with the pendant droplet, i.e., type-FA drop formation. For 5.6% HPC-sl solution, see also movie 1.

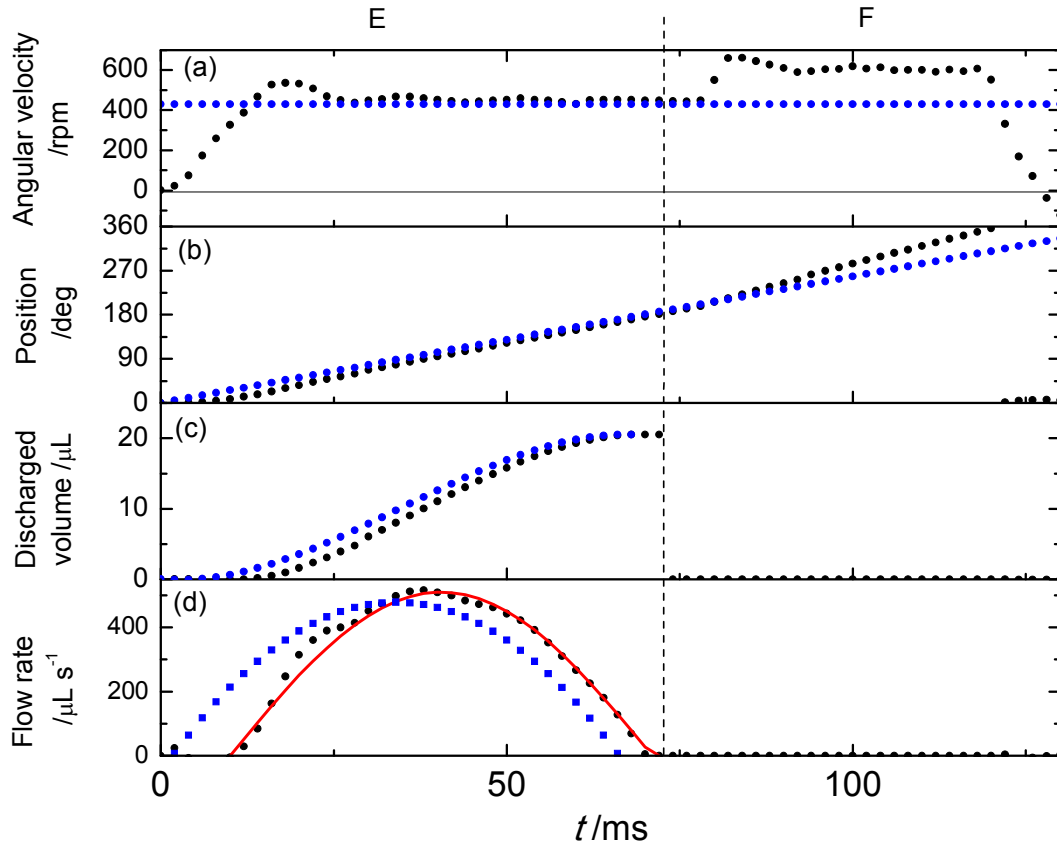


Figure 5. (Color online) Comparison of pump performance under a constant pump speed (blue dots) and one-step-ejection (OSE) DOD mode (black dots) shows (a) pump profile (angular velocity); (b) position feedback; (c) discharged volume; and (d) flow rate. The red line shows a sinusoidal fit to the flow rate in the OSE DOD process. E and F indicate ejection and filling phase, respectively.

Images, such as those shown in figure 6c, have been analysed to determine the variation in drop volume during the drop formation process. Figure 7 shows the evolution of the volume of the pendant droplet during the discharge phase (open black squares) until its detachment into a primary drop (open red triangle), along with the discharge volume from the pump (solid black squares). At the start of the pump discharge there is a small volume of fluid from the previous cycle; here the pendant drop has a volume of $2.7 \mu\text{L}$. The discharge from the pump is completed in approximately 65 ms, the drop starts necking under the forces of gravity and inertia from the ejected droplet. For this example it takes an additional 40 ms for a pendant drop to break fully into a primary drop, a satellite and a residual pendant drop.

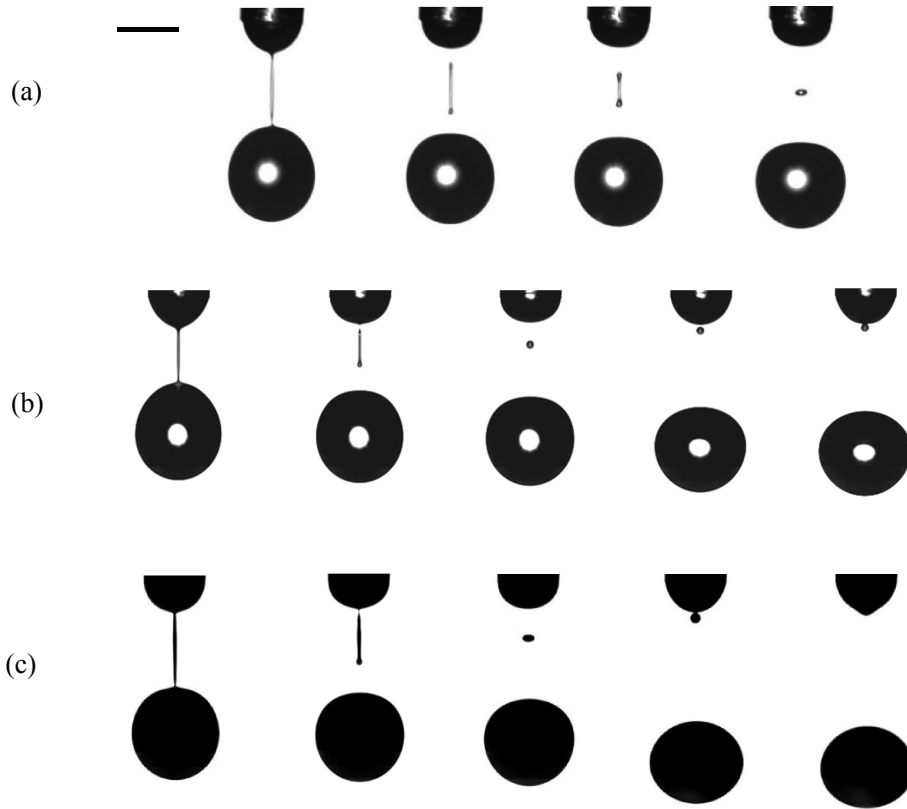


Figure 6. (a) Type-S drop formation of 5.6% HPC-sl/W under constant motor speed of 500 rpm. Time interval between images = 0.3 ms; (b) Type-FA drop formation of 5.6% HPC-sl/; and (c) Type-FA drop formation of AQ-20/W. (b) and (c) are under OSE pump cycle shown in figure 5. Time intervals between images in (b) and (c) are 1 ms, 1 ms, 4 ms and 1 ms from left to right. Scale bar is 2 mm.

By stroboscopic imaging, we observed over 100 drops 10 mm away from nozzle and noted that 70 satellites out of 111 did not merge with the pendant drop, which indicates the variability of the satellite drop. The variability is most likely to arise from inhomogeneities in the suspension changing the local fluid properties that influences the break-off and the kinetic energy in the satellite. In particular, the fluid can no longer be considered homogeneous when the ligament diameter approaches the length scale of the AQ crystals. Figure 8 illustrates the variation of the volume of satellite droplet for the AQ-20/W suspension as a function of ejection rate after discharging. At the critical point (ejection rate = 430 rpm), the satellite has a typical volume of $0.01 \mu\text{L}$ which is less than 0.1% of the primary drop of $18.6 \pm 0.2 \mu\text{L}$, obtained from imaging analysis. As the ejection rate increases, the satellite volume increases exponentially. A typical $0.2\text{-}\mu\text{L}$ satellite generated at the ejection rate of 650 rpm is 1% of the volume of

the primary drop. The uncertainty in the fate of deposition of a nanolitre drop will increase the risk of environmental contamination whilst a microlitre drop will degrade the uniformity of the primary drop size.

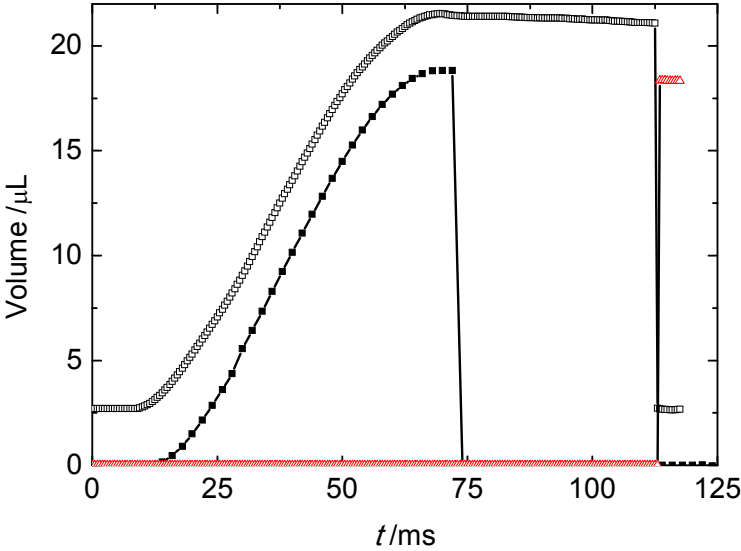


Figure 7. (Color online) Drop formation for AQ-20/W suspension under OSE DOD pump cycle shown in figure 5: the volumes of the pendant drop (open black squares), the pump discharge (solid black squares, from the encoder output), and detached drop (red triangle).

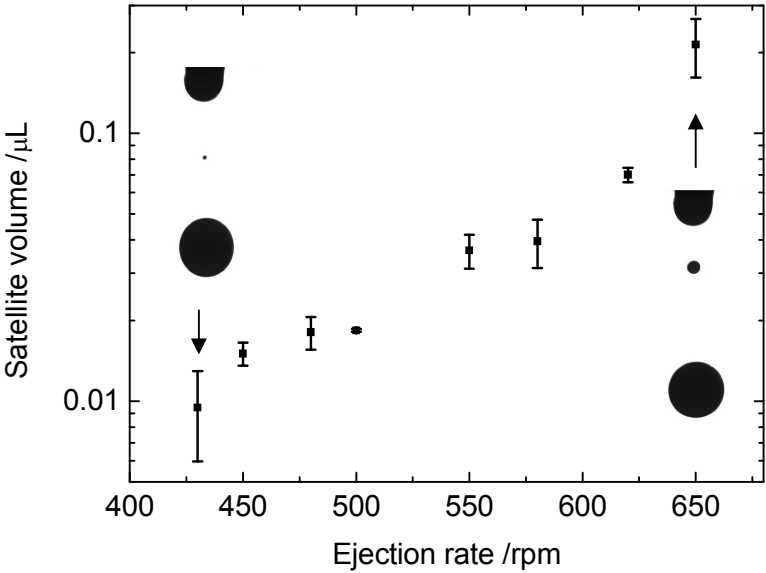


Figure 8. Satellite volume as a function of ejection rate in the OSE DOD pump cycle for AQ-20/W suspension. Type-FA. Stroke volume is 18.8 μL . Filling rate and acceleration and deceleration settings as in figure 5.

There are regions where satellite-free droplet formation does exist within the OSE pump cycle. Figure 9 shows an operability diagram as a function of stroke volume and ejection rate for the AQ-20/W suspension. There are three defined regions on this diagram. The one-drop multi-stroke regime exists where a single discharge of the pump is insufficient to eject a droplet from the nozzle. For example, if the ejection rate is less than 400 rpm for the stroke volume of 18.8 μL , multiple strokes are required to generate one drop. As the ejection rate is increased, the minimum pump volume required to eject a droplet is reduced, since the inertia of the ejected fluid is greater and can overcome the capillary and viscous forces that restrain droplet formation. Above this ejection critical point, one drop is formed with just one stroke. Within the one-stroke-one-drop range, the predominant droplet regime is overall type-FA break-off with the formation of a satellite. However there is a small region where just a single break-off of the capillary thread forms at the fore end of the ligament, i.e. type-F drop formation. The satellite-free region is illustrated in the area (Type-F in figure 9) enclosed by six experimental points established by scanning the ejection rate at constant stroke volume. The upper boundary is limited by the achievable stroke volume. The repeatability of the boundaries is typically ± 25 rpm.

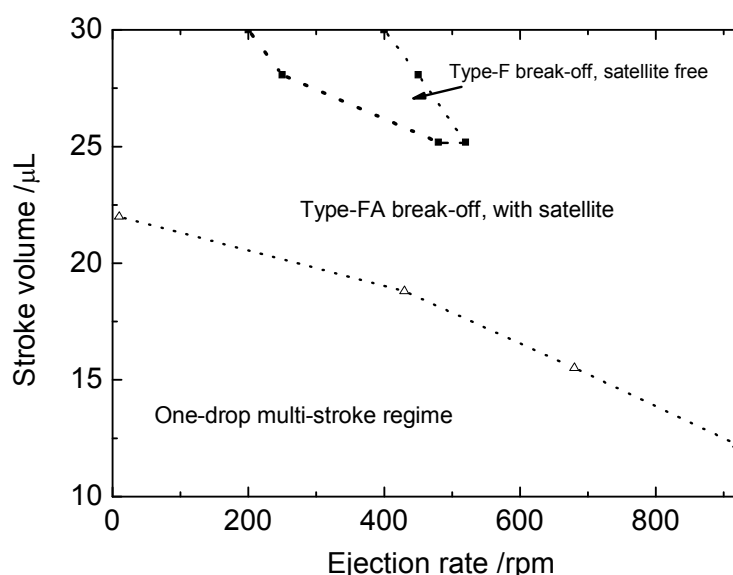


Figure 9. Operability window of AQ-20/W suspension in the OSE DOD pump cycle showing the region of type-FA (with satellite) and type-F (satellite-free) drop formation.

Figure 10 shows the evolution of type-F drop formation at an ejection rate of 300 rpm and a stroke volume of 28.0 μL while the conditions for filling, acceleration and deceleration remain the same as the DOD pump cycle in figure 5. The cone-shape ligament stretches to 6.6 mm and recoils back to the pendant drop. No satellite is formed. Type-F drop formation is typically seen in the dripping case, but is not shown in capillary jets according to the observations of Pimbley and Lee (Pimbley & Lee 1977).

The formation of satellite drops was also observed in 5.6%HPC-sl/water in a very similar manner to its non-Newtonian counterpart AQ-20/W, where both have a similar viscosity of at high shear rate of 1500 s^{-1} . Type-F drop formation was observed in this Newtonian fluid, shown in figure 1e (see also movie 5), under the same experimental condition of AQ-20/W shown in figure 10. For details of type-FA and type-S drop formation and break-off length as a function of ejection rate for this Newtonian fluid refer to Appendix A.

Since the operating window for satellite-free type-F drop formation is small, and the operating conditions give a long ligament and large pendant drop at the nozzle, it is not a practical drop generation approach in a liquid dispensing system. The next set of results describes a different approach to widen the operating window with the preferred type-A drop formation.

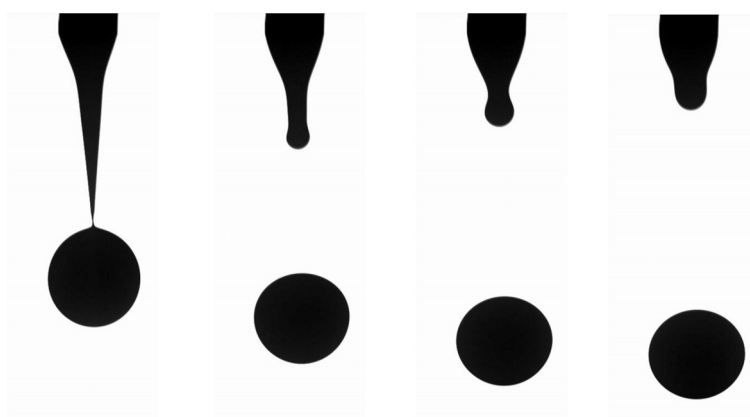


Figure 10. Satellite-free type-F drop formation in the OSE DOD pump cycle for AQ-20/W suspension. Images were obtained at intervals of 1.5 ms. Stroke volume is 28.0 μL .

4. Design of new pump cycle with the elimination of satellite drops

4.1 Introduction

Systems that generate satellite droplets are generally precluded from use in practical settings since the fate of the satellite droplet is unknown. With the single step ejection process described here the operating window is very narrow and a high degree of optimisation is required to find suitable fluid and operating parameters. The small operating window also limits the flexibility of the process with respect to drop volume and ejection speed. To widen the operating window, an alternative strategy was sought through controlling the inter-cycle flow profile over time. An additional degree of freedom is introduced by breaking the discharge of the pump into two parts with dwell time part way into the delivery of fluid from the nozzle. Figure 11 shows an example of the two-step-ejection (TSE) process highlighting the relationship between the rotational velocity of the pump, its position angular position, the discharged volume and the flow rate. The profile is divided into four phases: initial growth of the pendant droplet (G), pump filling over half a revolution (F), the ejection of the drop (E), and a dwell (D) after drop ejection. The growth and the ejection phases are each controlled by 3 parameters – the acceleration of the pump (G_a, E_a : rev/s²) to a constant angular velocity (G_v, E_v : rev/s) followed by the deceleration (G_d, E_d : rev/s²). The dwell phase is characterised by a time D_t . This rather long list of parameters, whilst offering a high degree of flexibility is not amenable to rational optimisation, but by recognising that the growth and fill phase are required to create a stable non-oscillating pendant droplet, then as long as the parameters G_a , G_v and G_d are not set so high as to eject a droplet, there are only 3 remaining parameters, E_a , E_v and E_d . Of these, the latter two are most closely associated with the ejection of the droplet and are ultimately the controlling parameters. Alongside, E_v and E_d , is the ratio of volumes of fluid delivered in the ejection and growth phases, expressed as $\alpha = V_E/V_G$, which is controlled by the piston position at the end of ejection phase. The stroke volume delivered by the pump completes the list of critical parameters. The key element of this new pump cycle is the ability to alter the pump flow profile at the end of ejection phase while the flow rate is high.

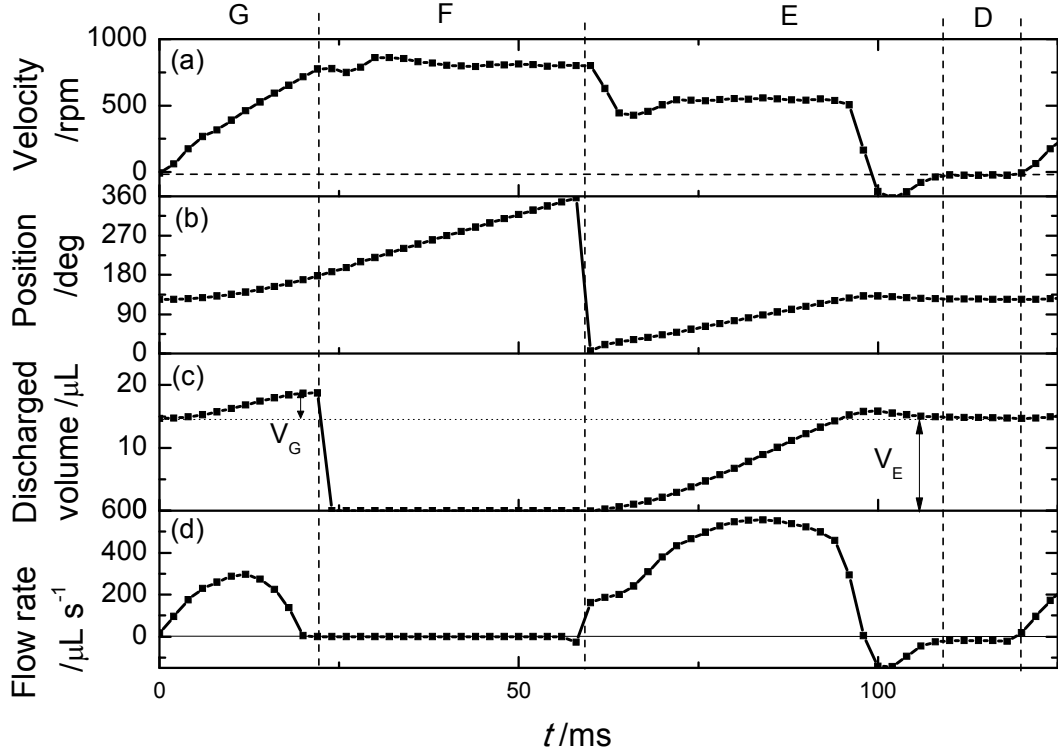


Figure 11. Two-step ejection process: (a) pump angular velocity profile, (b) position feedback, (c) discharged volume, (d) flow rate. In this example, different rotational velocities during the two steps have been specified ($G_v = 550$ rpm, $E_v = 500$ rpm) with a filling rate of 800 rpm. Acceleration and deceleration rates of 1000 rev s^{-1} are used throughout except for the deceleration after the first phase of ejection of 2000 rev s^{-1} . G, F, E and D indicate the process of the growth of the pendant drop, filling, ejection and dwell, respectively.

Figure 12 shows an example of the TSE process with the corresponding images of satellite-free drop formation with AQ-20/W. The starting point at $t = 0$ is a pendant drop of volume V_{res} ($= 0.7 \mu\text{L}$) remaining after break-off of the previous drop. This drop grows during through the growth phase (volume $V_G = 4.2 \mu\text{L}$) before the filling process occurs. G_v is chosen to prevent ejection of a small droplet, which has been observed at very high rates. During the fill time oscillations of the pendant drop damp out. The final addition of fluid occurs when a volume V_E is added ($= 14.6 \mu\text{L}$) to generate a primary drop of volume $V_E + V_G$ ($= 18.8 \mu\text{L}$) alongside the residual pendant droplet of volume V_{res} . In this case, $\alpha = V_E/V_G = 3.5$. The break-off of the primary droplet takes place about 20 ms after the fluid has stopped being pumped into the droplet and occurs through a combination of gravity, capillary forces and the momentum imparted by the

fluid leaving the nozzle and entering the droplet. In this example, the ligament breaks at the *aft* end and no satellite forms, i.e. type-A drop formation. The cycle then stops and will restart on an external trigger, giving a drop-on-demand operation.

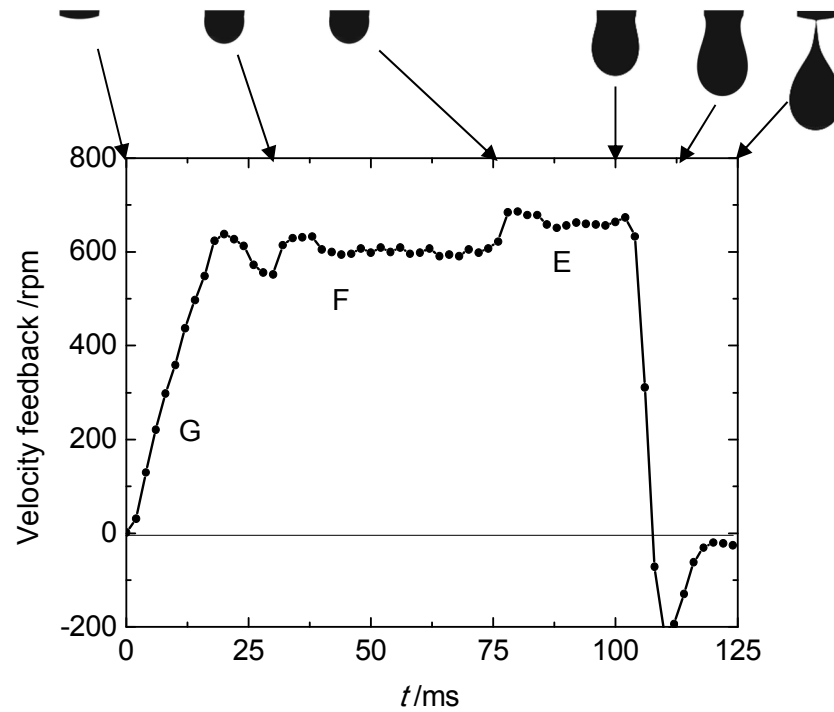
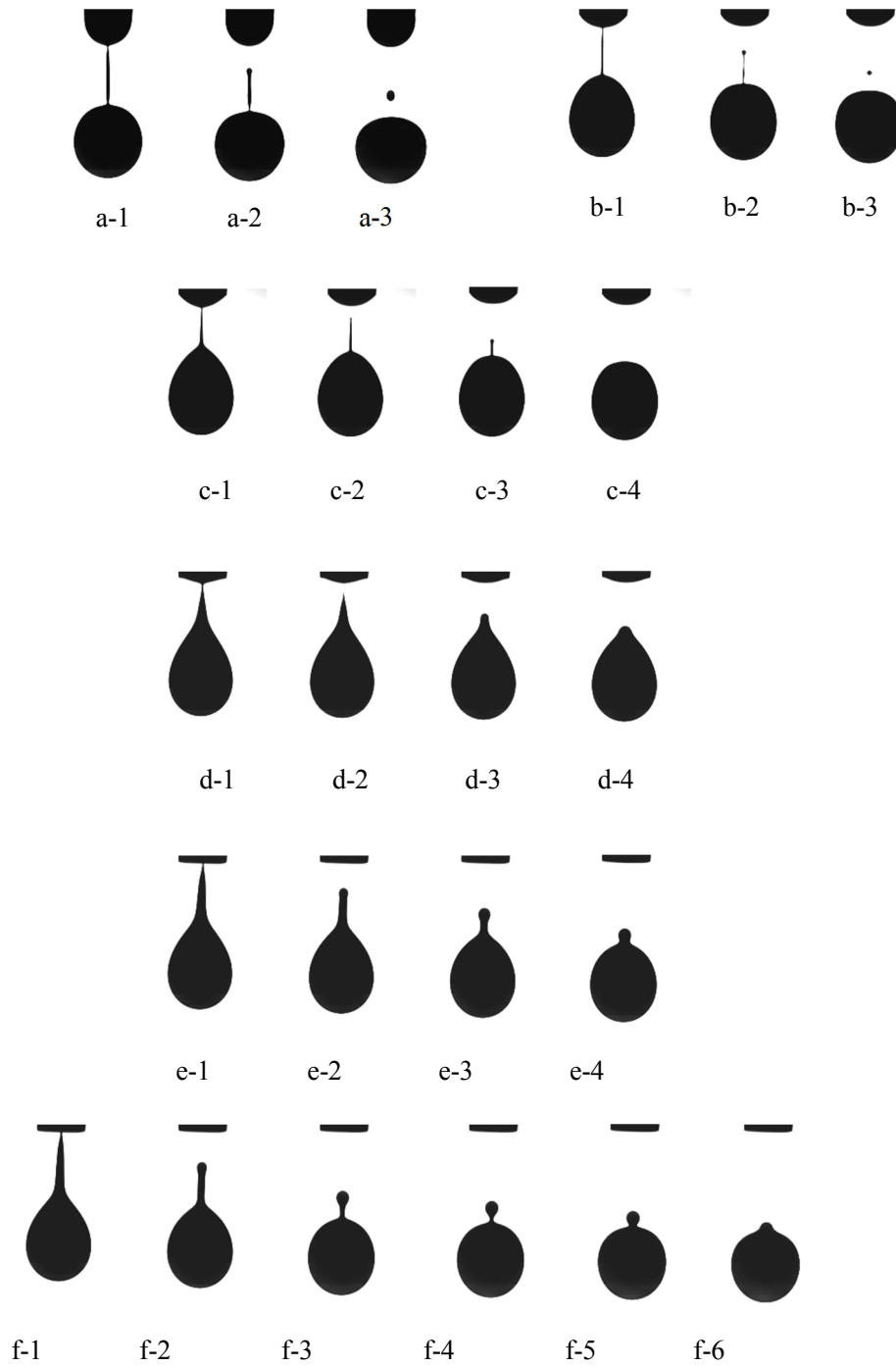


Figure 12. TSE process with the corresponding images of satellite-free drop formation with AQ-20/W. $E_v = 680$ rpm.

4.2 Effect of the ejection parameters on droplet formation

Figure 13 shows the range of droplet behaviour observed as a function of the pump speed during the ejection phase, E_v , with all other parameters held constant at the values shown in figure 11. There exists a lower speed of ejection below which the droplet does not eject from the nozzle. Beyond this there exists a transition in the type of breakup of AF→A→AF as the ejection rate E_v is increased from 450 rpm to 750 rpm. At the lowest ejection rate to generate one stroke one drop, a long, thin ligament forms and breaks off at the *aft* end first and then the *fore* end forming forward-merging satellite (type-AF drop formation), shown in figure 13a. As E_v increases to 580 rpm, the ligament gets shorter with a type-AF break-off and the residual drop and satellite get smaller, shown in figure 13b. At $E_v = 600$ rpm, the ligament is still thin but shorter with only one pinch-off at the *aft* end leading to a type-A break-off without a satellite, shown in figure 13c. Within the satellite-free window of $E_v = 600 - 740$ rpm, the ligament gets thicker as E_v

increases with a pronounced conical shape at the rear of the primary droplet and the residual drop becomes barely discernible (figure 13c–f). The ligament length reaches its minimum near $E_v = 660$ rpm (figure 13d). With a further small increase of E_v to 750 rpm, there is a transition from type-A to type-AF drop break-off. A large satellite appears and later on merges with the primary drop.



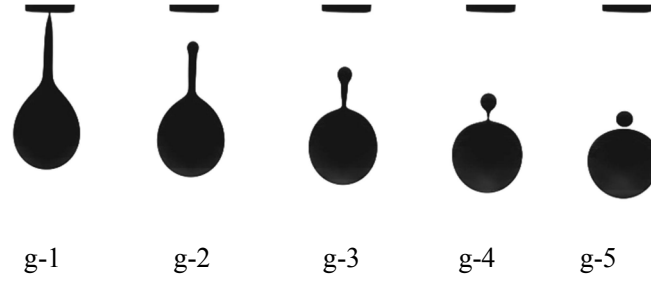


Figure 13. Transitions of the drop formation for AQ-20/W suspension in the TSE process with pump profile similar to that of figure 11 but with varied E_v of (a) 450 rpm at critical point; (b) 580 rpm (c) 600 rpm; (d) 660 rpm; (e) 720 rpm; (f) 740 rpm and (g) 750 rpm, with image time interval of (a) 1 ms; (b) 1 ms; (c) 0.5 ms; (d) 0.5 ms; (e) 1 ms; (f1-f3) 1.5 ms; (f3-f6) 0.5ms; and (g) 1.5 ms. Stroke volume is 18.8 μL .

The transition of drop formation illustrated above has also been observed in 5.6 wt% HPC-sl, shown in figure 1c (type-AF, see also movie 3) and figure 1d (type-A, see also movie 4), under similar pump parameters.

Figure 14 shows the break-off length as a function of E_v with the break-off type marked under the same condition as in figure 13. The minimum break-off length associated satellite-free drop formation corresponds to the ejection rate near the middle of the type-A operability window. Stroboscopic imaging was used to check the reproducibility of 400 droplets under the working conditions of figure 13d. The droplets were imaged at a distance from the nozzle of 10.1 ± 0.1 mm with a drop speed of 0.37 m s^{-1} . The mean drop volume analysed from images is $18.5 \mu\text{L}$ with a standard deviation of $0.1 \mu\text{L}$ which is believed a real measure of drop variability. No satellite was observed which demonstrates a high degree of repeatability of the droplet production process. For a fixed time delay between ejection and imaging, there is barely any perceivable difference in the droplet shape and position after break-off across multiple droplets. At the break-off there is a jitter of 2 pixels, i.e. maximum variation of $40 \mu\text{m}$ in the break-off length.

A second parameter associated with the ejection phase is the deceleration rate of the pump, E_d , at the end of the cycle. Figure 15a shows the change in the operating window for the cases of $\alpha = 1$ (circles) and 3.5 (squares), where $\alpha = V_E/V_G$. Other experimental parameters are as indicated in figure 11. As the deceleration rate decreases,

the operating window defined by the lower and upper values of E_v also reduces. The satellite-free window fully closes at deceleration rates below 600 rev s^{-2} for both $\alpha = 1$ and 3.5 . We note that with the slower deceleration (shown in figure 15b), the volume of fluid is added over a longer period (an extra 5 ms out of approximately 25 ms for the ejection) hence the momentum will be reduced.

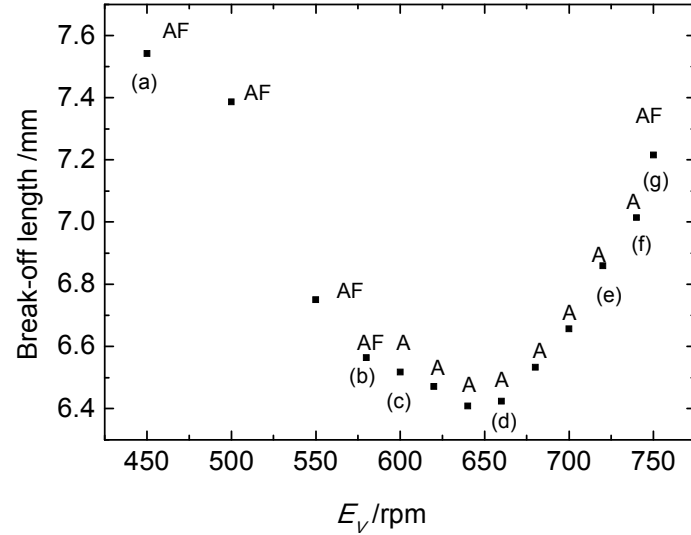


Figure 14. Break-off length as a function of E_v under the TSE process for AQ-20/W suspension. Labels A and AF indicate type-A or type-AF drop formation, respectively. Letters (a)-(g) corresponds to cases in figure 13.

4.3 Effect of the pump overshoot on drop formation

Rapid deceleration at the end of ejection phase (E) in TSE process leads to an overshoot in the pump position (as consequence of the PID control loop) causing the pump to reverse and suck liquid back into the pump chamber, shown in figure 16 profile-1. We therefore modified the pump profile to minimise the overshoot in the TSE process to study its effect on drop formation. We varied the ejection rate and set several deceleration steps near the end of ejection to avoid the overshoot, shown in figure 16 profile-2 and -3. For profile-3, the dwell between E and G is disabled in the motor command. The drop formation of sample 5.6% HPCsl/water under profile-1 with large overshoot is shown in figure 17a. Figure 17b corresponds to profile-2 with small overshoot and figure 16c to profile-3. While minimisation of the overshoot at the end of the ejection phase does not change the nature of type-A break-off, it does lead to a longer, thinner ligament, which is undesirable. The overshoot enhances type-A drop break-off. The most likely hidden information is that the larger the

overshoot the longer the interaction time between two possible pinch-offs (though of course this interaction time cannot actually be measured because the ligament recoils before the second pinch-off occurs).

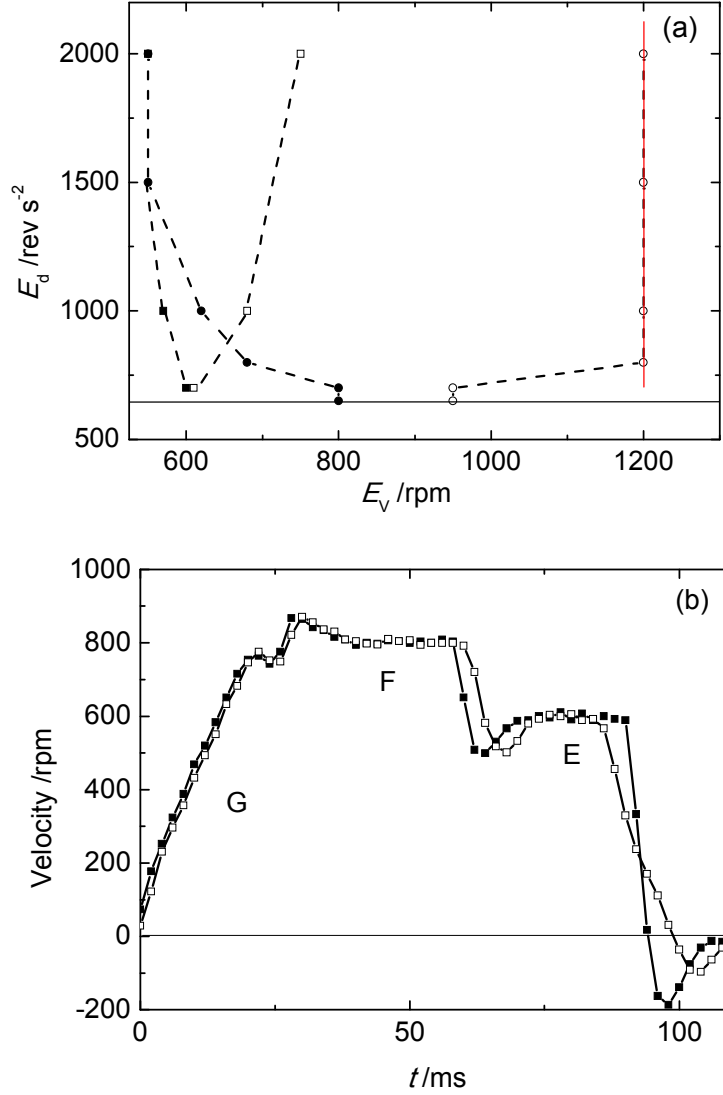


Figure 15. (Color online) (a) Deceleration-rate dependence of the satellite-free window for type-A drop break-off with $\alpha = 1$ (circles) and 3.5 (squares), respectively. Satellite-free region is confined within the solid and open symbols of the same type. Pump profile is similar to that of figure 12. Sample is suspension AQ-20/W. The solid black line shows the threshold of E_d above which satellite-free drop forms. Note that $E_v = 1200$ rpm (red line) represents the upper limit of measurements and not necessarily the limit of the operability from a fluid mechanical perspective. (b) Flow rate profile under different deceleration rate of E_d of 600 rev s^{-2} (open square) and 2000 rev s^{-2} (solid square) for $\alpha = 3.5$ and $E_v = 500 \text{ rev s}^{-1}$.

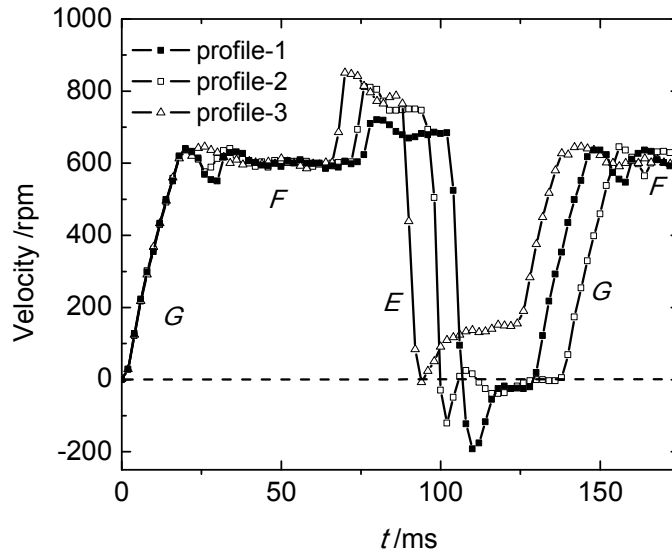


Figure 16. Three pump angular velocity profiles with the control of the overshoot at the end of ejection phase.

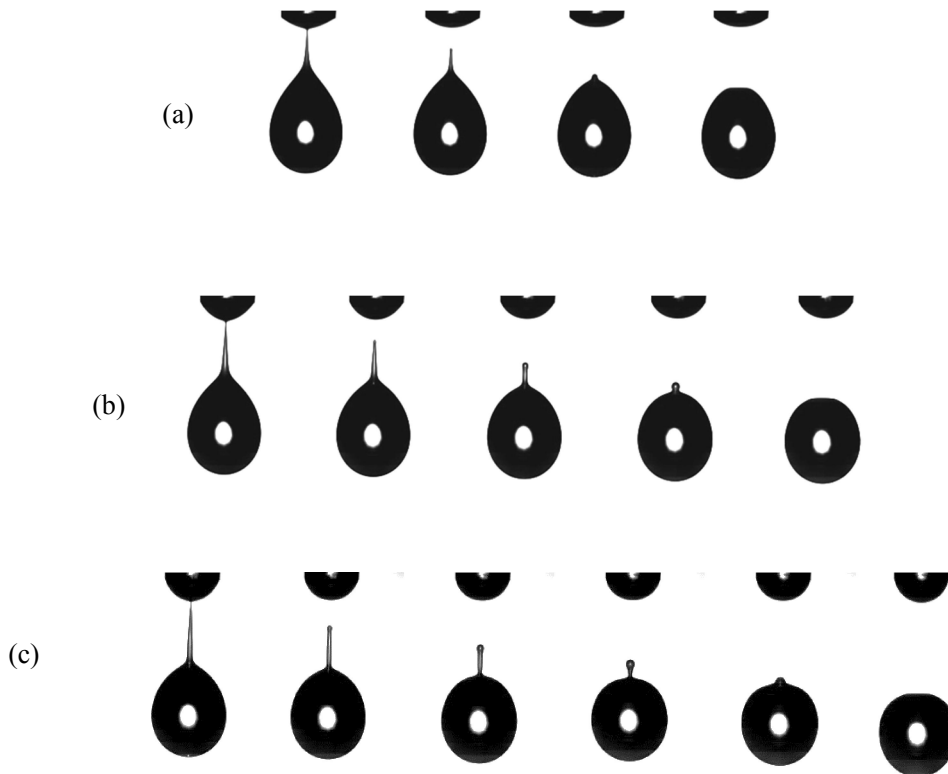


Figure 17. Type-A drop break-off under the TSE process with different pump overshoot at the end of ejection phase for 5.6% HPCsl/water. Drop formation is controlled under (a) profile-1, (b) profile-2 and (c) profile-3 in figure 16, respectively. All images have a time interval of 0.5 ms. $\alpha = 3.5$.

4.4 Effect of ratio of V_E / V_G on operability

Figure 18 shows the effect of α on the operating window for satellite-free formation (type-A) for AQ-20/W. The other conditions are as indicated in figure 11 but with varied E_v . For each stroke volume, there is a satellite-free region indicated between two dotted bounding lines. The triangular symbols are for $\alpha = 3.5$ and the circles for $\alpha = 1$; the filled symbols indicate the lower limit of the operating window and the open symbols the upper limit of the operating window. In addition the diagram is bounded by two solid lines, giving the minimum speed of the pump during phase E_v to effect ejection for one drop one stroke (open squares and black line), and an upper limit due to the maximum speed of the pump (red line). The smaller value of α provides a much larger operability window. However, a small value of α also results in a larger pendant drop which requires a longer time in the filling process to ensure that oscillations have fully damped out before the growth of the next droplet and smaller G_v to avoid its detachment from the nozzle.

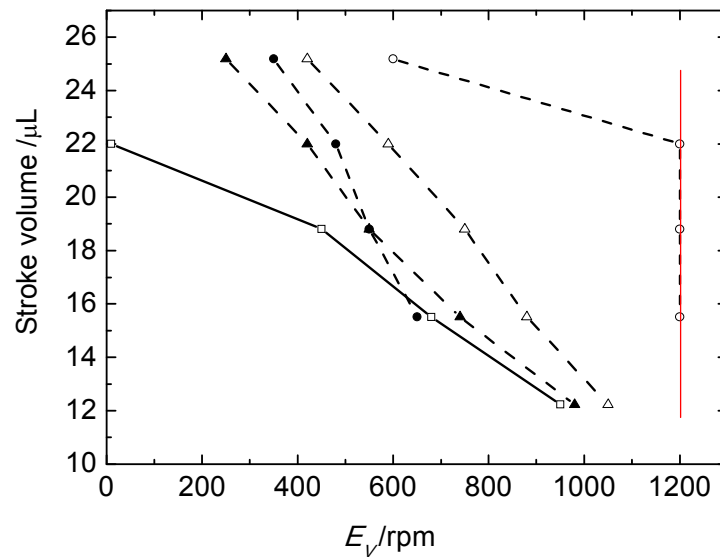


Figure 18. Satellite-free operability window in TSE process with pump profile similar to that of figure 11 but with varied E_v . For each stroke volume, there is a satellite-free region with confined E_v within the solid and open symbols (triangles for $\alpha = 3.5$ and circles for $\alpha = 1$, respectively). Open squares are critical points of E_v for each stroke volume. Note that $E_v = 1200$ rpm represents the upper limit of measurements (red line) and may not be the upper limit of the operability diagram.

5. Discussion

5.1 Viscosity effects on satellite-free drop formation

The effect of viscosity on satellite-free drop formation was studied by comparing the center of the satellite-free window among 4%, 5.6% and 6% HPC-sl solutions in water. The satellite-free window is shifted to higher E_v for the higher viscosity solutions, shown in figure 19.

For the non-Newtonian suspension of anthraquinone particles, we explored the upper limit on the weight fraction of AQ that could be successfully delivered as a satellite-free drop. Figure 20a shows drop formation for a 33 wt% suspension of AQ in water (AQ-33/W) under a constant pump speed of 480 rpm and with a stroke volume of 15 μL . The long ligament eventually splits into multiple satellites. Figure 20b shows the drop at its breakup under the two-step ejection profile, having a type-A drop formation without satellite.

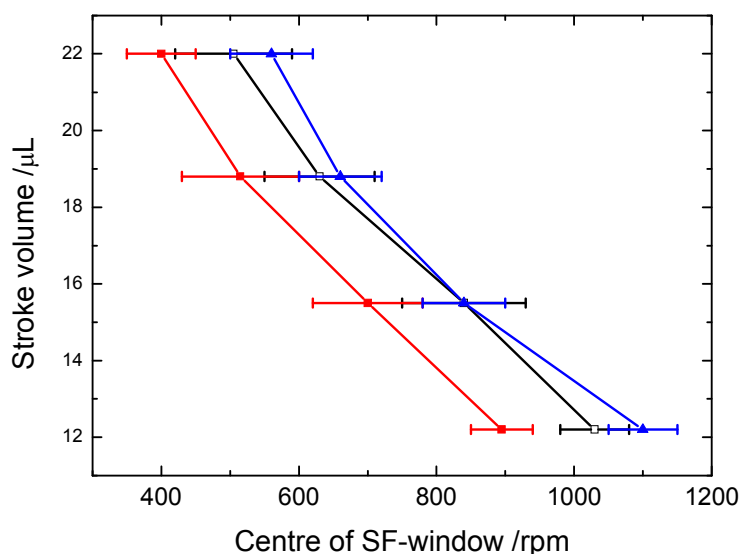


Figure 19. Centre of satellite-free (SF-) window of solution under TSE process with pump profile similar to that of figure 11 but with varied E_v for 4% (solid square, red), 5.6% (open square, black) and 6% HPC-sl solutions (triangle, blue). $\alpha = 3.5$. The bars indicate the extent of the operating window.

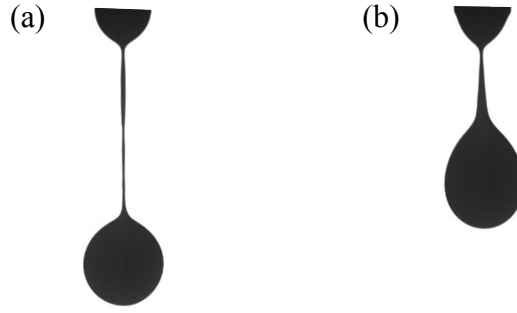


Figure 20. Discharge of a drop of AQ-33/W suspension with (a) a long ligament formed in the constant pump speed of 480 rpm and stroke volume 15 μL ; and (b) type-A drop formation under TSE with $E_v = 550$ rpm, $E_d = 2000$ rev s^{-2} , $\alpha = 1$, and stroke volume = 22.2 μL .

5.2 Shear rate inside the nozzle

To estimate the shear rate inside the pipe, we assume a parabolic flow. For a time-dependent flow rate (for example sinusoidal) with a maximum of Q_m of $500 \mu\text{L s}^{-1}$, (e.g. figure 5), we have the maximum velocity at the central pipe $U_0 \cong 4Q_m/(\pi^2 R^2)$. For the AWG15 nozzle that we used in the experiment, $R = 0.725$ mm and $U_0 \cong 0.4$ m s^{-1} . Therefore the maximum shear rate of $2U_0/R$ is 10^3 s^{-1} at the wall. Our Newtonian 5.6% HPC-sl/W solution was deliberately chosen to match the shear viscosity of suspension AQ-20/W at high shear rate of 1500 s^{-1} . We noted that in both OSE and TSE cases, the drop formation from these two fluids is similar under the same experimental condition. AQ-20/W is a shear-thinning fluid and so could display shear-banding or wall-slip, in which a central high-viscosity plug moves down the center of the tube and there is an annulus of high-shear, low-viscosity liquid near the walls. The fact that the fluid behaves as though it has the high-shear viscosity throughout the fluid suggests that these potential complexities in the fluid dynamics do not actually materialise – or at least do not adversely influence the drop formation process. A possible explanation is that all the fluid is exposed to high shear in the pump and the structure that gives rise to the yield stress does not have time to recover during the short period of time before ejection from the nozzle. We measured the dynamic surface tension and shear viscosity of suspension AQ-20/W immediately after drop formation by the oscillating drop method (Yang et al. 2014). The viscosity and dynamic surface tension of suspension

are similar to that of the polymer solution on the relevant timescales.

5.3 Dimensionless groups and characteristic times

Several non-dimensional parameters are commonly used to characterise the balance of inertial, surface tension, viscous and gravitational forces on the drop formation process: the Weber number We , Ohnesorge number Oh , capillary number Ca and Bond number Bo . These parameters are defined as

$$We = \frac{\rho D U^2}{\sigma}, \quad Oh = \frac{\mu}{\sqrt{\rho \sigma D}}, \quad Ca = \frac{\mu U}{\sigma}, \quad Bo = \rho g D^2 / \sigma,$$

where ρ is fluid density, σ is surface tension, D is the drop diameter, g is the gravitational acceleration and U is the mean flow velocity. The Ohnesorge and Bond numbers depend only on the fluid and the drop size. In our experiment, the stroke volume varies in the range 12–30 μL and drop diameter 2.8–3.8 mm. Oh lies between 0.05 (4%HPC) and 0.5 (AQ-33/W at a shear rate of 1500 s^{-1}). Bo is about 1.7–2.9. We note that the maximum volume of the pendant drop is estimated by the balance of capillary and gravitational forces, i.e. $V_{\max} = \sigma \pi D / (\rho g)$, where D is the diameter of the capillary tube. In our case pendant drop fully wets the nozzle plate, D is the outer diameter of the tube, i.e. 2.25 mm and we have $V_{\max} = 32 \mu\text{L}$. Thus for our experimental drop volume of 12 – 30 μL , the Worthington number (Berry et. al. 2015), which is defined as $Wo = V / V_{\max}$ and has the same physical meaning as Bond number, is in the range of 0.4 – 0.9.

The Weber and capillary numbers depend on the flow velocity, which is not constant through the DOD pump cycle. We estimate the mean flow velocity from the maximum flow rate Q_m by, $U \cong 2Q_m / (\pi^2 R^2)$, where R is the nozzle inner radius of 0.725 mm. For both OSE and TSE cases, shown in figure 5 and figure 11, respectively, the pump ejection rate E_v is about 600 rpm and the maximum flow rate is about 500 $\mu\text{L s}^{-1}$ which gives us mean flow velocity about 0.2 m s^{-1} (which is also the drop speed near the end of ejection) and $We \sim 3$ and $Ca \sim 0.1$ for the given fluid and drop size.

From the operability window of AQ-20/W suspension in the OSE (figure 9) and

TSE processes (figure 18), we see that the We and Ca numbers have the same order of magnitude in both cases. However, we have shown that the variation of the time-dependent flow profile can have a pronounced effect on drop formation. The typical times for the break-off of a 18.8- μL primary droplet are about 40 ms for OSE and 20 ms for TSE after the fluid has stopped being pumped into the droplet. The characteristic timescale for drop pinch-off at the neck is the capillary time, $\sqrt{\frac{\rho R^3}{\sigma}}$, which is about 10 ms under our experimental condition. For a pendant drop there are also capillary and gravity-driven oscillations, with time periods of $2\pi\sqrt{\frac{\rho R^3}{8\sigma}}$ and $2\pi\sqrt{\frac{5R}{4g}}$, respectively (Lamb 1881). Under our experimental condition, these timescales are 17–25 ms and 84–95 ms, respectively. Therefore the oscillation of the large primary drop due to capillary forces may play a role in stretching the fine ligament between the primary and residual drop, but the gravitational force does not.

6. Conclusions

We have described a drop-on-demand liquid dispensing system based on a piston pump with precise control of discharged volume in the range 12–30 μL . We observed five types of drop breakup with both Newtonian and Non-Newtonian fluids studied in the paper, depending mainly on the temporal profile of the flow profile. We identified a persistent satellite problem and a very narrow satellite-free operating window under a conventional one-step-ejection process. A novel pump profile was designed in which the drop is ejected in two steps and this profile was applied to aqueous model suspensions and polymer solutions. The satellite drop can be eliminated within a wide operability window over a range of viscosity of the sample. The key factors that affect the formation of satellite-free droplets under the designed TSE profile, with the key physical requirement for satellite-free type-A drop break-off, is a rapid deceleration in the flow rate near its maximum. Such a rapid deceleration cannot be achieved in the one-step profile owing to the sinusoidal form of the flow profile during the ejection cycle. This satellite-free DOD liquid dispensing system has a potential application in

pharmaceutical manufacturing and other dispensing applications where precise delivery of viscous fluids with volumes in the microliter range is required.

Acknowledgement

We acknowledge the support of the TSB (grant number BD352J). We thank Dr. David Hoyle (Durham University) for helpful discussions on the rheology measurements.

Appendix A. drop formation of 5.6%HPC-sl/W solution under the OSE DOD process

Figure 21 shows the drop break-off length increases as the ejection rate for 5.6%HPC-sl/W with the stroke volume of $18.8 \mu\text{L}$. The pump setting is the same as that for its non-Newtonian counterpart, described in figure 8. The break-off length is defined as the distance between nozzle plate and first pinch-off. For the studied pump stroke, HPC drop breaks off mostly in type-FA mode except that in the case of ejection rate of 670 rpm the ligament breaks simultaneously at both ends (shown in figure 1b and movie 2), i.e. type-S mode.

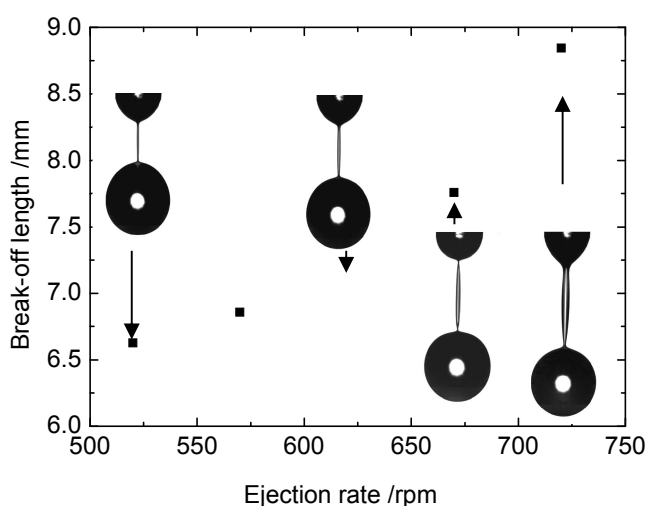


Figure 21. Break-off length as a function of ejection rate under DOD pump cycle (the same as figure 8) for 5.6%HPC-sl/water, showing a monotonic increase with ejection rate. Stroke volume is $18.8 \mu\text{L}$.

References

- Basaran, O.A., 2002. Small-scale free surface flows with breakup: Drop formation and emerging applications. *AIChE Journal*, 48(9), 1842–1848.
- Beecher, P. et al., 2007. Ink-jet printing of carbon nanotube thin film transistors. *Journal of Applied Physics*, 102(4), 1–7.
- Berry, J. D., Neeson, M. J., Dagastine, R. R., Chan, D. Y. C., Tabor, R. F., 2015. Measurement of surface and interfacial tension using pendant drop tensiometry. *J. Colloid Interface Sci.* 454, 226–237
- Castrejón-Pita, J.R., Martin, G.D., Hoath, S.D. & Hutchings, I.M., 2008. A simple large-scale droplet generator for studies of inkjet printing. *Review of Scientific Instruments*, 79(7), 075108.
- Castrejón-Pita, J.R., Morrison, N.F., Harlen, O.G., Martin, G.D. & Hutchings, I.M., 2011. Experiments and Lagrangian simulations on the formation of droplets in drop-on-demand mode. *Physical Review E - Statistical, Nonlinear, and Soft Matter Physics*, 83(3), 1–12.
- Castrejón-Pita, J.R., Willis, S.J. & Castrejón-Pita, A.A., 2015. Dynamic nozzles for drop generators. *Review of Scientific Instruments*, 86(11), 1–6.
- Chaudhary, K.C. & Maxworthy, T., 1980. The nonlinear capillary instability of a liquid jet. Part 3. Experiments on satellite drop formation and control. *Journal of Fluid Mechanics*, 96, 287–297.
- Clarke, A., Fiesser, F., Yang, L., Bain, C.D. & Kapur, N., 2013. Liquid dispensing device and methods of control the same. *Patent application 61/790508 USA*.
- Dong, H., Carr, W.W. & Morris, J.F., 2006. An experimental study of drop-on-demand drop formation. *Physics of Fluids*, 18(7), 072102.
- Eggers, J., 1997. Nonlinear dynamics and breakup of free-surface flows. *Reviews of Modern Physics*, 69(3), 865–930.
- Eggers, J., 2005. Drop formation - an overview. *Z. Angew. Mech.* 85(6), 400–410
- Fromm, J., 1984. Numerical calculation of the fluid dynamics of drop-on-demand jets. *IBM J. Res. Dev.* 28(3), 322–333
- Gamerith, S., Klug, A., Scheiber, H., Scherf, U., Moderegger, E. & List, E.J.W., 2007. Direct ink-jet printing of Ag-Cu nanoparticle and Ag-precursor based electrodes for OFET applications. *Advanced Functional Materials*, 17(16), 3111–3118.
- Harris, D. M., Liu, T. and Bush, J. W. M., 2015. A low-cost, precise piezoelectric droplet-on-demand generator. 56(83), 1950–6
- Kwon, K.-S., 2010. Experimental analysis of waveform effects on satellite and ligament behavior via in situ measurement of the drop-on-demand drop formation curve and the instantaneous jetting speed curve. *Journal of Micromechanics and Microengineering*, 20(11), 115005.
- Kyser, E.L. & Sears, S.B., 1976. Method and apparatus for recording with writing fluids and

877 drop projection means therefor. US3946398A.

878 Lamb, H., 1881. On the Oscillations of a Viscous Spheroid. *Proc. Lond. Math. Soc.* 1, 51-70

879 Martin, G.D., Hoath, S.D. & Hutchings, I.M., 2008. Inkjet printing - the physics of
880 manipulating liquid jets and drops. *Journal of Physics: Conference Series*, 105, 012001.

881 Ng, T.N., Lujan, R.A., Sambandan, S., Street, R.A., Limb, S. & Wong, W.S., 2007. Low
882 temperature a-Si:H photodiodes and flexible image sensor arrays patterned by digital
883 lithography. *Applied Physics Letters*, 91(6), 89–92.

884 Pimbley, W.T. & Lee, H.C., 1977. Satellite Droplet Formation in a Liquid Jet. *IBM Journal of*
885 *Research and Development*, 21(1), 21–30.

886 Subramani, H.J., Yeoh, H.K., Suryo, R., Xu, Q., Ambravaneswaran, B. & Basaran, O.A., 2006.
887 Simplicity and complexity in a dripping faucet. *Physics of Fluids*, 18(3), 032106.

888 Sumerel, J., Lewis, J., Doraiswamy, A., Deravi, L.F., Sewell, S.L., Gerdon, A.E., Wright, D.W.
889 & Narayan, R.J., 2006. Piezoelectric ink jet processing of materials for medical and
890 biological applications. *Biotechnology Journal*, 1, 976–987.

891 Wang, X., Carr, W.W., Bucknall, D.G. & Morris, J.F., 2012. Drop-on-demand drop formation
892 of colloidal suspensions. *International Journal of Multiphase Flow*, 38(1), 17–26.

893 Xu, Q. and Basaran, O. A., 2007. Computational analysis of drop-on-demand drop formation.
894 *Phys. Fluids*, 19, 102111

895 Yang, L., Kazmierski, B.K., Hoath, S.D., Jung, S., Hsiao, W.-K., Wang, Y., Berson, A., Harlen,
896 O., Kapur, N. & Bain, C.D., 2014. Determination of dynamic surface tension and viscosity
897 of non-Newtonian fluids from drop oscillations. *Physics of Fluids*, 26(11), 113103.

898 Zoltan, S.I., 1972. Pulsed droplet ejection system. US3683212A.